Parallel 3-d simulations of a twophasic porous media model in spinemechanics

W. Ehlers[1], N. Karajan[1], and C. Wieners[2]

[1] Institute of Applied Mechanics (Civil Engineering),
Universität Stuttgart, Pfaffenwaldring 7, 70569 Stuttgart, Germany
[2] Institute for Applied and Numerical Mathematics,
Universität Karlsruhe, Englerstr. 2, 76 128 Karlsruhe, Germany

Abstract. This contribution presents an extended model based on the Theory of Porous Media (TPM), which is suitable for the simulation of electro-chemically active soft tissues and, in particular, the intervertebral disc (IVD). The respective non-linear constitutive equations include the modelling of the anisotropic material behaviour as well as the osmotic pressure. We introduce a stable finite element discretization, and we propose an iterative parallel solution method with a domain decomposition preconditioner combining an algebraic coarse grid solver on an overlay mesh and approximate ILU solving on the subdomains. Finally, the efficiency of the model is shown by a fully coupled 3-d simulation of a lumbar spine (vertebrae L1 to L5), where one computation shows a healthy spine segment while the other one includes a stiffened L4-L5 motion segment.

1 Introduction

For a better understanding of the complex coupled behaviour of the IVD and its influence on the overall performance of the spine, an appropriate finite element model describing all relevant effects would be of great benefit. In this context, such a model will remarkably aid the design of new implants, if it is possible to reproduce a realistic response due to external loads. However, a realistic numerical simulation of such a complex biological structure requires not only an elaborated material model but also an efficient solution method for the discretized system.

The spine itself consists of several vertebrae and intervertebral discs embedded in between. In our model we neglect the cartilaginous endplates separating the discs and the vertebrae since we expect that their mechanical behaviour is of minor importance. Two main regions can be distinguished in an axial cut through the IVD: a gelatinous core, the nucleus pulposus (NP), enclosed by a fibrous, lamellar structure, the anulus fibrosus (AF). Both regions are composed of a porous multi-component microstructure consisting of a charged, hydrated extracellular matrix as well as an ionized interstitial fluid, yielding a active swelling material. Herein, the solid skeleton consists of proteoglycans (PG's), glycosaminoglycans (GAG's), and collagen fibres of type I and II saturated by a liquid containing dissolved anions and cations

as solutes. The large PG's and GAG's are thereby trapped in the collagen network and carry negative fixed charges, which therefore underlie the same motion as the whole solid matrix. For more details see, e. g., [1, 7, 14, 17] and references therein.

Due to the porous microstructure of both the IVD and the vertebrae, these materials can be adequately modelled in the framework of the TPM. The respective constitutive equations, needed to capture all occurring phenomena, are implemented and can be switched on and off via material parameters. Furthermore, several inhomogeneities occur in the IVD. In particular, this is the inhomogeneous distribution of the orientation and mechanical behaviour of the collagen fibres in the AF as well as the concentration of the fixed negative charges. These inhomogeneities are captured as is described in [7].

The arising coupled set of governing equations can be reformulated in variational form which then allows for a discrete approximation by finite elements. We use Taylor-Hood elements with quadratic approximations of the solid displacement and linear pressure approximation, since they provide stable results also for small time steps and for a wide range of Darcy parameters.

For a full simulation of several spine segments, a sufficiently fine geometry resolution is essential. This leads to very large algebraic systems, so that reliable numerical computations cannot be performed on single processor machines. Thus, a parallel finite element implementation is used, where parallel Krylov methods are used together with a strong preconditioner for the solution of the linearized problems. The efficiency of this solution method is then demonstrated by numerical results showing the mechanical response of vertebrae and intervertebral discs under loading forces. Herein, two computations are performed, one concerning a healthy lumbar spine and another having the lowest motion segment, i. e., the L4-L5 segment, stiffened.

2 An extended binary porous media model

In a standard incompressible biphasic model for quasi-static processes with no mass exchange between the constituents and negligible body forces, the respective volume and momentum balances read

$$\operatorname{div}\left[\,(\mathbf{u}_S)'_S + n^F\,\mathbf{w}_F\right] = 0 \qquad \text{and} \qquad \operatorname{div}\left(\mathbf{T}^S + \mathbf{T}^F\right) = \mathbf{0}\,, \tag{1}$$

cf. [4]. In this context, the porosity of the model is denoted by n^F with its counterpart $n^S = 1 - n^F$ representing the solidity. The seepage velocity is denoted by $\mathbf{w}_F$, whereas $(\mathbf{u}_S)'_S$ is the material time derivative of the solid displacement vector with respect to the deforming solid skeleton. The overall stress of the model $\mathbf{T} = \mathbf{T}^S + \mathbf{T}^F$ is the sum of the partial Cauchy stress tensors of the solid and the fluid constituent, respectively.

Following this, the partial stress tensors are subjected to the principle of effective stresses (cf. [3, 16]) yielding a split into hydrostatic and so-called extra quantities

$$\mathbf{T}^S = -n^S\,p_{\mathrm{hyd}}\,\mathbf{I} + \mathbf{T}^S_E \qquad \text{and} \qquad \mathbf{T}^F = -n^F\,p_{\mathrm{hyd}}\,\mathbf{I} + \mathbf{T}^F_E\,, \tag{2}$$

where $\mathbf{I}$ denotes the second-order identity tensor. As is usual in hydraulics, the fluid extra stress $\mathbf{T}_E^F$ is neglected due to dimensional reasons, cf. [11]. In order to capture the soft tissues swelling capability, osmotic effects have to be incorporated using a further split

$$\mathbf{T}_E^S = -p_{\mathrm{osm}}\,\mathbf{I} + \mathbf{T}_{E,\mathrm{mech}}^S \tag{3}$$

of the solid extra stress into osmotic and purely mechanical contributions. Thus, the overall pressure is given by $p_{\mathrm{tot}} = p_{\mathrm{hyd}} + p_{\mathrm{osm}}$. In this context, p_{osm} models the colloid osmotic pressure and is understood as the pressure difference between the internal osmotic pressure, which results from the concentrations of the NaCl-solutes and the fixed negative charges, and the external osmotic pressure arising from the NaCl-solutes of the fluid surrounding the tissue. Due to Lanir's assumption [10] stating that the dissolved ions and cations move very rapidly and do not generate concentration gradients in the tissue, van't Hoff's osmotic law

$$p_{\mathrm{osm}} = R\Theta\left[\sqrt{4\,\bar{c}_m^{\,2} + (c_m^{fc})^2} - 2\,\bar{c}_m\right] \tag{4}$$

can be applied to the whole domain and is not restricted to the boundary. Herein, R is the universal gas constant, Θ denotes the absolute temperature, $\bar{c}_m$ is the molar concentration of the solutes in the surrounding (external) fluid, and c_m^{fc} is the molar concentration of the fixed negative charges with respect to the fluid volume inside the tissue. Hence, the latter quantity is deformation dependent, as volumetric deformations in the tissue directly influence the volume fraction n^F of the fluid. If a local concentration balance is postulated and integrated from initial quantities $(\,\cdot\,)_{0S}$, cf. [6], the relation

$$c_m^{fc} = c_{0S}^{fc}\, n_{0S}^F\, (J_S - n_{0S}^S)^{-1}\,, \qquad \text{where} \qquad J_S = \det \mathbf{F}_S\,, \tag{5}$$

can be derived for the change of the concentration of the fixed charges. As a consequence, $(5)_1$ depends on the solid Jacobian J_S measuring the volumetric deformation of the overall tissue.

Further constitutive assumptions concern the purely mechanical solid extra stress. We proceed from the idealization of an hyperelastic solid skeleton, which must be capable of capturing the isotropic extracellular matrix as well as the anisotropic fibre reinforcements resulting from the collagen fibres of Type I. Following [6], the resulting isotropic and anisotropic Cauchy stresses can be expressed in a decoupled manner as

$$\begin{aligned}
\mathbf{T}_{E,\mathrm{mech}}^S &:= \mathbf{T}_{E,\mathrm{iso}}^S + \mathbf{T}_{E,\mathrm{aniso}}^S\,, \qquad \text{where} \\
\mathbf{T}_{E,\mathrm{iso}}^S &= \frac{\mu_0^S}{J_S}(\,\mathbf{F}_S\,\mathbf{F}_S^T - \mathbf{I}\,) + \Lambda_0^S (1 - n_{0S}^S)^2 \Big(\frac{1}{1 - n_{0S}^S} - \frac{1}{J_S - n_{0S}^S}\Big)\,\mathbf{I}\,, \\
\mathbf{T}_{E,\mathrm{aniso}}^S &= \frac{\tilde{\mu}_1^S}{J_S}\, I_4^{-1}(\, \tilde{I_4^{\gamma_1^S}}{}^{/2} - 1\,)\,(\mathbf{a}\otimes\mathbf{a}) + \frac{\tilde{\mu}_1^S}{J_S}\, I_6^{-1}(\, \tilde{I_6^{\gamma_1^S}}{}^{/2} - 1\,)\,(\mathbf{b}\otimes\mathbf{b})\,.
\end{aligned} \tag{6}$$

Here, μ_0^S is the classical ground-state shear modulus, Λ_0^S is the second Lamé constant, $\tilde{\mu}_1^S$ and $\tilde{\gamma}_1^S$ are parameters concerning the mechanically equivalent behaviour of the collagen fibre families, where $\mathbf{a} = \mathbf{F}_S\,\mathbf{a}_0$ and $\mathbf{b} = \mathbf{F}_S\,\mathbf{b}_0$ are the fibre directions in the deformed configuration with given constant unit fibre directions $\mathbf{a}_0$ and $\mathbf{b}_0$ in the reference frame. The corresponding mixed invariants $I_4 = \mathbf{a}\cdot\mathbf{a}$ and $I_6 = \mathbf{b}\cdot\mathbf{b}$ describe the squared stretches in the respective fibre direction. Finally, the set of independent unknowns in the process is reduced by Darcy's filter law

$$n^F\,\mathbf{w}_F = -\frac{K_{0S}^S}{\mu^{FR}}\,\operatorname{grad} p_{\mathrm{hyd}}\,, \tag{7}$$

which is inserted into $(1)_1$. The parameters K_{0S}^S and μ^{FR} of (7) are the intrinsic permeability coefficient and the effective dynamic viscosity of the fluid, respectively, and $\operatorname{grad}(\,\cdot\,)$ denotes the gradient with respect to the location vector $\mathbf{x}$ of the deformed configuration.

3 Weak formulation of the binary model

For the computational model, an interval in time $[0,T]$ and a reference domain $\Omega = \Omega_0 \subset \mathbb{R}^3$ is fixed. The primary variables are the solid displacement $\mathbf{u}_S$ and the hydrostatic pressure p_{hyd}. For a given displacement vector $\mathbf{u}_S$, the deformed configuration is denoted by $\Omega(\mathbf{u}_S)$, and the solid deformation gradient on $\Omega(\mathbf{u}_S)$ is computed via its inverse $\mathbf{F}_S^{-1} = \mathbf{I} - \operatorname{grad}\mathbf{u}_S$.

Data. A specific configuration is determined by the following data: the reference domain Ω_0, appropriate load functionals defining traction forces $\bar{\mathbf{t}}$ and the fluid efflux $\bar{q}$, and essential boundary conditions for

$$\begin{aligned} \mathbf{u}_S(t,\mathbf{x}) &= \mathbf{u}_S^D(t,\mathbf{x})\,, \qquad \mathbf{x} \in \Gamma_S(t) \subset \partial\Omega_t\,, \\ p_{\mathrm{hyd}}(t,\mathbf{x}) &= p_{\mathrm{hyd}}^D(t,\mathbf{x})\,, \qquad \mathbf{x} \in \Gamma_F(t) \subset \partial\Omega_t\,, \end{aligned} \tag{8}$$

on some parts of the boundary (using $\Omega_t = \Omega(\mathbf{u}_S(t))$). Due to the choice of p_{hyd} as primary variable, the model does not a priori exhibit a stress-free reference configuration. This becomes clear when (3) to (6) are combined in order to compute the overall stress of the model, thereby using values of the natural state, i. e., $\mathbf{u}_S = \mathbf{0}$ and $p_{\mathrm{hyd}} = 0$. Due to (4), there is always an initial osmotic pressure

$$p_{\mathrm{osm,OS}} = R\Theta\left[\sqrt{4\,\bar{c}_m^{\,2} + (c_{0S}^{fc})^2} - 2\,\bar{c}_m\right]. \tag{9}$$

Hence, the constant part $p_{\mathrm{osm,OS}}\,\mathbf{I}$ is added onto the mechanical extra stress $(6)_1$ to enforce a stress free reference configuration in the sense of classical continuum mechanics. Note that without this modification, the model would describe an initial swelling of the tissue until equilibrium between the (9) and

the tension in the mechanical extras stress $(6)_1$ is reached. As this contribution is concerned with numerical solution strategies, the described simpler approach by directly starting with the initial osmotic pressure (9) is used here.

Finally, the model also depends on several material parameters. For a full set of suitable parameters please refer to Table 1 in Section 5.

Variational formulation. With these settings, it is now possible to state the full biphasic problem at time $t \in [0,T]$: for a given traction vector $\bar{\mathbf{t}}$ and a given efflux $\bar{q}$ of the interstitial fluid find $\mathbf{u}_S$ and p_{hyd} satisfying the essential boundary conditions and the balance equations in weak form

$$\begin{aligned} \int_{\Omega_t} \mathbf{T}^S_{E,\mathrm{mech}} \cdot \operatorname{grad} \mathbf{v} \; \mathrm{d}v - \int_{\Omega_t} p_{\mathrm{tot}} \operatorname{div} \mathbf{v} \; \mathrm{d}v \qquad &= \int_{\partial\Omega_t} \bar{\mathbf{t}} \cdot \mathbf{v} \; \mathrm{d}a \,, \\ \int_{\Omega_t} \operatorname{div} (\mathbf{u}_S)'_S \, q \; \mathrm{d}v + \int_{\Omega_t} \frac{K^S_{0S}}{\mu^{FR}} \operatorname{grad} p_{\mathrm{hyd}} \cdot \operatorname{grad} q \; \mathrm{d}v &= \int_{\partial\Omega_t} \bar{q} \, q \; \mathrm{d}a \end{aligned} \tag{10}$$

for all test functions $\mathbf{v}$ and q satisfying $\mathbf{v} = \mathbf{0}$ on $\Gamma_S(t)$ and $q = 0$ on $\Gamma_F(t)$. Here, $\mathbf{T}^S_{E,\mathrm{mech}}$ depends (non-linearly) on the deformation gradient, and p_{tot} depends on its determinant.

For simplicity, the abbreviations $\mathbf{u} = \mathbf{u}_S$ and $p = p_{\mathrm{hyd}}$ are used in the following.

Discretization in time. For a given time series $0 = t_0 < t_1 < t_2 < \cdots < T$, the backward Euler method reads as follows: for a given $\mathbf{u}^{n-1}$ depending on $\Delta t_n = t_n - t_{n-1}$, $\bar{\mathbf{t}}_n = \bar{\mathbf{t}}(t_n)$ and $\bar{q}_n = \bar{q}(t_n)$, the unknowns $\mathbf{u}^n$ and p^n of the time step n are computed satisfying the essential boundary conditions

$$\begin{aligned} \mathbf{u}^n(\mathbf{x}) &= \mathbf{u}^D_S(t_n, \mathbf{x}) \,, \qquad && \mathbf{x} \in \Gamma^n_S := \Gamma_S(t_n) \,, \\ p^n(\mathbf{x}) \; &= p^D_{\mathrm{hyd}}(t_n, \mathbf{x}) \,, \qquad && \mathbf{x} \in \Gamma^n_F := \Gamma_F(t_n) \,, \end{aligned} \tag{11}$$

and

$$\begin{aligned} R^n_S(\mathbf{u}^n, p^n)[\mathbf{v}] &= 0 \,, \qquad && \text{for all } \mathbf{v} \text{ with } \mathbf{v} = \mathbf{0} \text{ on } \Gamma^n_S, \\ R^n_F(\mathbf{u}^n, p^n)[q] &= 0 \,, \qquad && \text{for all } q \text{ with } q = 0 \text{ on } \Gamma^n_F, \end{aligned} \tag{12}$$

where the residuals are given by

$$\begin{aligned} R^n_S(\mathbf{u}, p)[\mathbf{v}] &= \int_{\Omega(\mathbf{u})} \mathbf{T}^S_{E,\mathrm{mech}}(\operatorname{grad} \mathbf{u}) \cdot \operatorname{grad} \mathbf{v} \, \mathrm{d}v \\ &\quad - \int_{\Omega(\mathbf{u})} \left[p + p_{\mathrm{osm}}(\operatorname{grad} \mathbf{u}) \right] \operatorname{div} \mathbf{v} \, \mathrm{d}v - \int_{\partial\Omega(\mathbf{u})} \bar{\mathbf{t}}_n \cdot \mathbf{v} \; \mathrm{d}a \,, \\ R^n_F(\mathbf{u}, p)[q] &= - \int_{\Omega(\mathbf{u})} \operatorname{div} (\mathbf{u} - \mathbf{u}^{n-1}) \, q \; \mathrm{d}v \\ &\quad - \Delta t_n \int_{\Omega(\mathbf{u})} \frac{K^S_{0S}}{\mu^{FR}} \operatorname{grad} p \cdot \operatorname{grad} q \; \mathrm{d}v + \Delta t_n \int_{\partial\Omega(\mathbf{u})} \bar{q}_n \, q \; \mathrm{d}a \; . \end{aligned} \tag{13}$$

Discretization in space. In the special case of small deformations and $\Delta t_n \, K^S_{0S}/\mu^{FR} \approx 0$, the incremental problem is close to a saddle point problem: Compute $\mathbf{w}$ and r satisfying

$$\begin{aligned} &\int_\Omega (\mathbb{C} \operatorname{grad} \mathbf{w}) \cdot \operatorname{grad} \mathbf{v} \; \mathrm{d}v - \int_\Omega r \operatorname{div} \mathbf{v} \; \mathrm{d}v = -R_S[\mathbf{v}] \,, \\ &- \int_\Omega \operatorname{div} \mathbf{w} \, q \; \mathrm{d}v \qquad\qquad\qquad\qquad\qquad\quad = -R_F[q] \end{aligned} \tag{14}$$

for all $\mathbf{v}$ with $\mathbf{v} = \mathbf{0}$ on Γ^n_S and q with $q = 0$ on Γ^n_F. This system has the same structure as the Stokes system. Thus, in order to avoid oscillations, a stable discretization $\mathbf{u}_h \in \mathbf{V}_h$ and $p_h \in Q_h$ satisfying the inf-sup condition

$$\sup_{\mathbf{v}_h \neq 0} \frac{\displaystyle\int_\Omega q_h \operatorname{div} \mathbf{v}_h \; \mathrm{d}v}{\displaystyle\Big(\int_\Omega \mathbb{C} \operatorname{grad} \mathbf{v}_h \cdot \operatorname{grad} \mathbf{v}_h \; \mathrm{d}v \Big)^{1/2}} \geq \; \beta \, \Big(\int_\Omega q_h^2 \; \mathrm{d}v \Big)^{1/2} \tag{15}$$

for all $q_h \in Q_h$ with $\int_\Omega q_h \, \mathrm{d}v = 0$ has to be used, where β is a constant which is independent of the mesh width. In this context, numerically stable Taylor-Hood elements ($\mathrm{Q}_2/\mathrm{Q}_1$) are applied with isoparametric 20-node bricks for the displacements $\mathbf{u}$ and trilinear pressure p, see [2].

Consistent Newton iteration. In every time step, choose suitable start iterates $\mathbf{u}^{n,0}$ and $p^{n,0}$ satisfying the essential boundary conditions (11), and for $k = 1, 2, 3, ...$ compute increments $\mathbf{w}$ and r (with homogeneous boundary conditions on the Dirichlet boundary parts) by solving the linearized variational problem of the form

$$\begin{aligned} a^{n,k}_{SS}(\mathbf{w}, \mathbf{v}) + a^{n,k}_{FS}(r, \mathbf{v}) &= -R^n_S(\mathbf{u}^{n,k-1}, p^{n,k-1})[\mathbf{v}] \,, \\ a^{n,k}_{SF}(\mathbf{w}, q) + a^{n,k}_{FF}(r, q) \; &= -R^n_F(\mathbf{u}^{n,k-1}, p^{n,k-1})[q] \,, \end{aligned} \tag{16}$$

for all test functions $\mathbf{v}$ and q with homogeneous boundary conditions on the Dirichlet boundary parts. The bilinear forms $a^{n,k}_{SS}(\cdot,\cdot)$ and $a^{n,k}_{FS}(\cdot,\cdot)$ are the derivatives of $R^n_S(\cdot)$ with respect to the solid and the fluid component at $(\mathbf{u}^{n,k}, p^{n,0})$, and $a^{n,k}_{SF}(\cdot,\cdot)$, $a^{n,k}_{FF}(\cdot,\cdot)$ are the derivatives of $R^n_F(\cdot)$.

Then, a suitable damping factor $s^{n,k} \in (0, 1]$ is determined such that for the updated variables

$$\begin{aligned} \mathbf{u}^{n,k} &= \mathbf{u}^{n,k-1} + s^{n,k} \, \mathbf{w} \,, \\ p^{n,k} \; &= p^{n,k-1} + s^{n,k} \, r \end{aligned} \tag{17}$$

the residual norm is decreasing. If no such damping parameter is found, the time increment Δt_n is reduced. Close to the solution of the incremental problem it is expected that no damping is necessary, i. e., $s^{n,k} = 1$.

4 A parallel linear solver

The porous media model is realized in the FEM research software PANDAS [5, 15], and a parallel front end for assembling and solving the system is provided by M++ (see [18, 19] for details on the parallel programming model and for the definition of general interfaces). The main feature of this software is a geometry-based data structure relying on the concept of distributed objects, where every object is associated to a geometric point. In particular, the unknowns are associated to their nodal points. This allows for a transparent realization of the parallel consistency requirements for the finite element solution along the parallel interface.

Within the non-linear and time-dependent simulation, the most sensible part of the parallelization is the solution of the linear problems within every Newton step. Here, we use a parallel GMRES method, as is described in [19], together with a domain decomposition preconditioner.

From numerical experiments it is well-known that overlapping domain decomposition preconditioners with coarse grid correction applied to the Stokes system with Taylor-Hood elements are very efficient, see [8, 9]. Hence, this type of preconditioning is a good choice for the discussed application to complex bio-mechanical structures, although two major modifications are required due to the following reasons: Only a moderate number of processors is used so that the subdomain problems are too large for exact solving. Moreover, the underlying geometry is too complex to allow for a small coarse mesh. Thus, an inexact sub-domain solver is used (a multilevel ILU with pivoting and dropping strategy by Mayer [12, 13]) and the coarse problem is constructed on an independent overlay mesh.

Altogether, this preconditioner can easily be constructed within the parallel interface, i. e., it requires only algebraic and geometric information and it is, thus, fully decoupled from the modelling and finite element discretization provided by PANDAS.

5 Numerical experiments

For the numerical application to the human lumbar spine we use the material model described in section 2 with three different sets of parameters listed in Table 1. Herein, the vertebrae are considered as a homogeneous uncharged hard tissue, thereby neglecting its original structure consisting of a dense cortical shell and a soft spongiosa inside. Furthermore, the AF and NP of the IVD are modelled with all occurring inhomogeneities as is described in [6]. In this context, the parameters addressing the mechanical behaviour of the collagen fibres are only given at selected points, i. e., at internal and external regions in dorsal and ventro-lateral positions, which are needed for a linear interpolation in the AF.

The presented initial boundary value problems concern a lumbar spine with removed processes, one having healthy IVD's and another having the

lowest motion segment stiffened, i. e., the lowest IVD behaves like a vertebra. Moreover, all free surfaces are drained ($p_{\mathrm{hyd}} = 0$), the lower surface of the L5-vertebra is totally fixed in space ($\mathbf{u}_S = \mathbf{0}$), and the top surface of the L1-vertebra is loaded with the traction vector $\bar{\mathbf{t}}$, which results in a vertical (F_V) and horizontal (F_H) force when integrated over the surface. The traction vector is then linearly increased with time, until the healthy and the stiffened lumbar spine show a tip deflection of 54.3 mm. The corresponding tip-loads are $F_V = 85\,\mathrm{N}$, $F_H = 21\,\mathrm{N}$ and $F_V = 108\,\mathrm{N}$, $F_H = 27\,\mathrm{N}$ with loading times $t = 0.201\,\mathrm{s}$ and $t = 0.255\,\mathrm{s}$ for the healthy and the stiffened spine, respectively. Results of the 3-d simulation are depicted in Figure 1 showing the total pressure in the sagittal plane of the spine.

Vertebrae: Treated with no distinction between cortical shell and spongiosa.			
$n^S_{0S} = 0.2$	[-]	$K^S_{0S} = 2.7 \cdot 10^{-5}$	[mm^2]
$c^{fc}_{0S} = 0.0$	[mol/mm^3]	$\mu^{FR} = 3.8 \cdot 10^{-8}$	[Ns/mm^2]
$\mu^S_0 = 192.0$	[MPa]	$\Lambda^S_0 = 225.7$	[MPa]
Nucleus Pulposus: Treated as isotropic and charged material.			
$n^S_{0S} = 0.3$	[-]	$K^S_{0S} = 3.5 \cdot 10^{-12}$	[mm^2]
$c^{fc}_{0S} = 0.3 \cdot 10^{-6}$	[mol/mm^3]	$\mu^{FR} = 6.9 \cdot 10^{-10}$	[Ns/mm^2]
$\mu^S_0 = 0.5$	[MPa]	$\Lambda^S_0 = 0.75$	[MPa]
Anulus Fibrosus: Treated as inhomogeneous anisotropic charged material.			
$n^S_{0S} = 0.3$	[-]	$K^S_{0S} = 6.2 \cdot 10^{-12}$	[mm^2]
$c^{fc}_{0S} = 0.1 \cdot 10^{-6}$	[mol/mm^3]	$\mu^{FR} = 6.9 \cdot 10^{-10}$	[Ns/mm^2]
$\mu^S_0 = 0.95$	[MPa]	$\Lambda^S_0 = 2.2$	[MPa]

	Ventro-Lat. Int.	Ventro-Lat. Ext.	Dorsal Int.	Dorsal Ext.
$\tilde{\mu}^S_1$ [MPa]	0.0343	0.1463	0.0059	0.0508
$\tilde{\gamma}^S_1$ [-]	44.051	97.135	30.464	54.239

Table 1. Material parameters of the biphasic model for the vertebrae, nucleus pulposus and anulus fibrosus, respectively.

The lumbar spine was discretized using 72 320 20-node Taylor-Hood elements yielding a total of 982 044 degrees of freedom. The computations were carried out in parallel on the cluster "Leonardo da Vinci" of the Institute of Applied Mechanics (CE) at the Universität Stuttgart, using 84 CPU's (2.2 GHz Opterons with 1 GB RAM/CPU). The full simulation time was 5:44 [h:min] and 11:32 [h:min] for the healthy and the stiffened spine, respectively. In both computations a fixed time increment $\Delta t_n = 0.003\,\mathrm{s}$ is used.

As expected, the force which is required to accomplish the same deformation with the stiffened lumbar spine is remarkably higher than the force needed for the healthy lumbar spine. Moreover, the maximum total intradiscal

pressure p_{tot} in the L3-L4 disc is also raised from 0.7 MPa to 1.0 MPa comparing the healthy with the stiffened state. Note that this is even a higher value than the 0.95 MPa of total disc-pressure reached in the healthy L4-L5 disc. Hence, it is obvious that the stiffening of a motion segment causes a surplus load in the adjacent IVD, when deformations are kept constant.

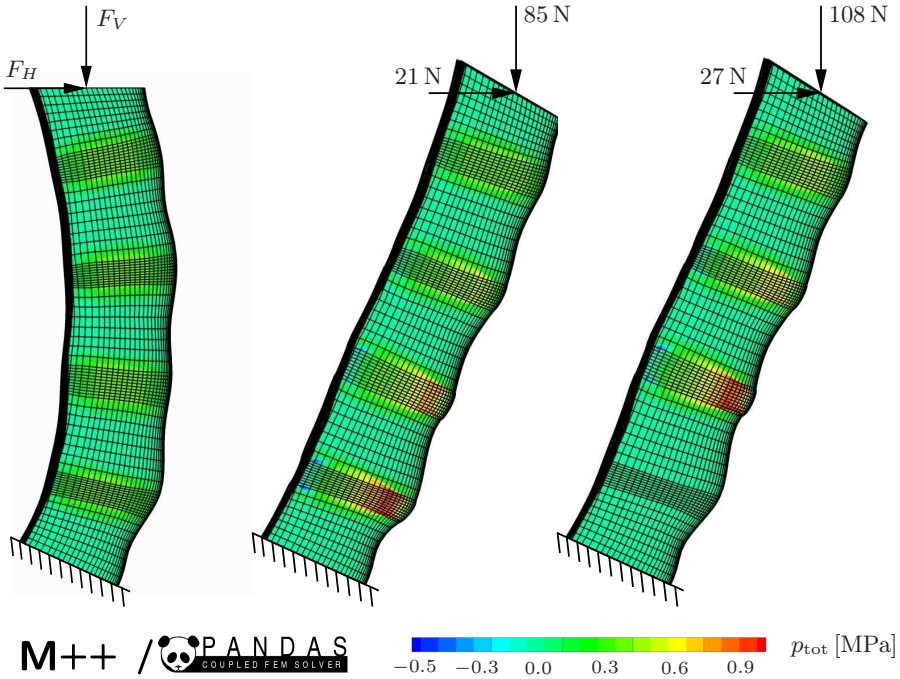

Fig. 1. Sagittal cut illustrating the load-deformation behaviour and the total pressure development inside the IVD's for a healthy lumbar spine (middle) and one having the L4-L5 motion segment stiffened (right). The reference configuration is shown on the left.

References

1. Ayad, S. & Weiss, J. B.: Biochemistry of the intervertebral disc. In Jayson, M. I. V. (ed.): *The Lumbar Spine and Back Pain*, 3rd ed., Churchill Livingstone, New York 1987, pp. 100–137.
2. Brezzi, F. & Fortin, M.: *Mixed and Hybrid Finite Element Methods*. Springer-Verlag, Berlin 1991.
3. Ehlers, W.: Constitutive equations for granular materials in geomechanical context. In Hutter, K. (ed.): *Continuum Mechanics in Environmental Sciences and Geophysics*, CISM Courses and Lectures No. 337, Springer-Verlag, Wien 1993, pp. 313–402.

4. Ehlers, W.: Foundations of multiphasic and porous materials. In Ehlers, W. & Bluhm, J. (eds.): *Porous Media: Theory, Experiments and Numerical Applications*, Springer-Verlag, Berlin 2002, pp. 3–86.
5. Ehlers, W. & Ellsiepen, P.: PANDAS: Ein FE-System zur Simulation von Sonderproblemen der Bodenmechanik. In Wriggers, P.; Meißner, U.; Stein, E. & Wunderlich, W. (eds.): *Finite Elemente in der Baupraxis: Modellierung, Berechnung und Konstruktion*, Beiträge zur Tagung FEM '98 an der TU Darmstadt am 5. und 6. März 1998, Ernst & Sohn, Berlin 1998, pp. 391–400.
6. Ehlers, W.; Karajan, N. & Markert, B.: A porous media model describing the inhomogeneous behaviour of the human intervertebral disc. *Materials Science and Engineering Technology* **37** (2006), 546–551.
7. Ehlers, W.; Markert, B. & Karajan, N.: A coupled FE analysis of the intervertebral disc based on a multiphasic TPM formulation. In Holzapfel, G. A. & Ogden, R. W. (eds.): *Mechanics of Biological Tissue*, Springer, Berlin 2006, pp. 373–386.
8. Klawonn, A. & Pavarino, L. F.: Overlapping Schwarz methods for mixed linear elasticity and Stokes problems. *Computer Methods in Applied Mechanics and Engineering* **165** (1998), 233–245.
9. Klawonn, A. & Pavarino, L. F.: A comparison of overlapping Schwarz methods and block preconditioners for saddle point problems. *Numerical Linear Algebra with Applications* **7** (2000), 1–25.
10. Lanir, Y.: Biorheology and fluid flux in swelling tissues. I. Bicomponent theory for small deformations, including concentration effects. *Biorheology* **24** (1987), 173–187.
11. Markert, B.: *Porous media viscoelasticity with application to polymeric foams.* Dissertation, Bericht Nr. II-11 aus dem Institut für Mechanik (Bauwesen), Universität Stuttgart 2005.
12. J. Mayer. A multilevel crout ilu preconditioner with pivoting and row permutation. *Numer. Linear Algebra Appl.*, 2007. to appear.
13. J. Mayer. Symmetric permutations for I-matrices to delay and avoid small pivots. *SIAM J. Sci. Comp.*, 2007. to appear.
14. Mow, V. C. & Hayes, W. C.: *Basic orthopaedic biomechanics.* Lippincott-Raven, New York 1997.
15. PANDAS: Porous media Adaptive Non-linear finite element solver based on Differential Algebraic Systems. `http://www.get-pandas.com`
16. Skempton, A. W.: Significance of Terzaghi's concept of effective stress (Terzaghi's discovery of effective stress). In Bjerrum, L.; Casagrande, A.; Peck, R. B. & Skempton, A. W. (eds.): *From Theory to Practice in Soil Mechanics*, Wiley, New York 1960, pp. 42–53.
17. Urban, J. P. G. & Roberts, S.: Intervertebral disc. In Comper, W. D. (ed.): *Extracellular Matrix, Volume 1, Tissue Function*, Harwood Academic Publishers GmbH 1996, pp. 203–233.
18. Wieners, C.; Ammann, M. & Ehlers, W.: Distributed point objects: A new concept for parallel finite elements applied to a geomechanical problem. *Future Generation Computer Systems* **22** (2006), 532–545.
19. Wieners, C.; Ammann, M.; Ehlers, W. & Graf, T.: Parallel Krylov methods and the application to 3-d simulations of a tri-phasic porous media model in soil mechanics. *Computational Mechanics* (2005) **36**, 409–420.